

Size- and shape-dependent pleural translocation, deposition, fibrogenesis, and mesothelial proliferation by multiwalled carbon nanotubes

Jiegou Xu,^{1,2} David B. Alexander,¹ Mitsuru Futakuchi,³ Takamasa Numano,³ Katsumi Fukamachi,³ Masumi Suzui,³ Toyonori Omori,⁴ Jun Kanno,⁵ Akihiko Hirose⁶ and Hiroyuki Tsuda¹

¹Laboratory of Nanotoxicology Project, Nagoya City University, Nagoya, Japan; ²Department of Immunology, Anhui Medical University College of Basic Medical Sciences, Hefei, China; ³Department of Molecular Toxicology, Nagoya City University Graduate School of Medical Sciences, Nagoya; ⁴Air Environment Division Environment Management Bureau, Ministry of the Environment, Government of Japan, Tokyo; ⁵Divisions of Cellular and Molecular Toxicology; ⁶Risk Assessment, National Institute of Health Sciences, Tokyo, Japan

Key words

Fibrosis, mesothelial proliferation, multiwalled carbon nanotubes, parietal pleura, pleural inflammation

Correspondence

Hiroyuki Tsuda, Laboratory of Nanotoxicology Project, Nagoya City University, 3-1 Tanabedohri, Mizuho-ku, Nagoya 467-8603, Japan.
Tel: +81-52-836-3496; Fax: 81-52-836-3497;
E-mail: htsuda@phar.nagoya-cu.ac.jp

Funding Information

Health and Labour Sciences Research Grants of Japan; Princess Takamatsu Cancer Research Fund.

Received January 28, 2014; Revised April 10, 2014;
Accepted April 29, 2014

Cancer Sci 105 (2014) 763–769

doi: 10.1111/cas.12437

Multiwalled carbon nanotubes (MWCNT) have a fibrous structure similar to asbestos, raising concern that MWCNT exposure may lead to asbestos-like diseases. Previously we showed that MWCNT translocated from the lung alveoli into the pleural cavity and caused mesothelial proliferation and fibrosis in the visceral pleura. Multiwalled carbon nanotubes were not found in the parietal pleura, the initial site of development of asbestos-caused pleural diseases in humans, probably due to the short exposure period of the study. In the present study, we extended the exposure period to 24 weeks to determine whether the size and shape of MWCNT impact on deposition and lesion development in the pleura and lung. Two different MWCNTs were chosen for this study: a larger sized needle-like MWCNT (MWCNT-L; $l = 8 \mu\text{m}$, $d = 150 \text{ nm}$), and a smaller sized MWCNT (MWCNT-S; $l = 3 \mu\text{m}$, $d = 15 \text{ nm}$), which forms cotton candy-like aggregates. Both MWCNT-L and MWCNT-S suspensions were administered to the rat lung once every 2 weeks for 24 weeks by transtracheal intrapulmonary spraying. It was found that MWCNT-L, but not MWCNT-S, translocated into the pleural cavity, deposited in the parietal pleura, and induced fibrosis and patchy parietal mesothelial proliferation lesions. In addition, MWCNT-L induced stronger inflammatory reactions including increased inflammatory cell number and cytokine/chemokine levels in the pleural cavity lavage than MWCNT-S. In contrast, MWCNT-S induced stronger inflammation and higher 8-hydroxydeoxyguanosine level in the lung tissue than MWCNT-L. These results suggest that MWCNT-L has higher risk of causing asbestos-like pleural lesions relevant to mesothelioma development.

Pleural plaque and malignant mesothelioma are characteristic lesions in asbestos-exposed humans and usually originate from the parietal pleura.^(1,2) Properties of asbestos fibers, including dimension, chemical composition, surface reactivity, durability and biopersistence, asbestos deposition-induced oxidative stress and inflammation, and simian virus 40 infection have all been implicated in the pathogenesis of pleural diseases, especially malignant mesothelioma.^(3,4)

High concentrations of asbestos fibers have been found in the black spots of the parietal pleura⁽⁵⁾ and detected in pleural plaques and malignant mesothelioma⁽⁶⁾ in asbestos-exposed patients, suggesting that deposition of asbestos fibers in the parietal pleura is an early event and plays an important role in the pathogenesis of pleural lesions. However, why parietal pleura are the initial and preferential targets of asbestos is not known. According to an explanatory paradigm suggested by Donaldson *et al.*,⁽⁷⁾ a fraction of the fibers in the lung are routinely transported into the pleural cavity through unidentified routes. Unlike spherical particles and short fibers, long fibers cannot be cleared effectively through the stomata (small holes

in the parietal pleura), resulting in the long fibers being trapped and deposited in the parietal pleura. This deposition causes pro-inflammatory, genotoxic, and mitogenic responses in the deposition sites.⁽⁷⁾

Carbon nanotubes have a fibrous structure with a high aspect ratio. This structural feature, shared with asbestos, raises concern that widespread use of carbon nanotubes may lead to asbestos-like diseases in exposed humans.^(8,9) Multiwalled carbon nanotubes (MWCNT) directly injected into the peritoneal cavity or the scrotum in rodents induce mesothelial lesions, including malignant mesothelioma,^(10–13) suggesting that inhaled MWCNT may lead to pleural plaque and mesothelioma if fibers enter the pleural cavity. Furthermore, MWCNT administered to the lung has been found to translocate into the pleural cavity and induce inflammation in the pleural cavity and mesothelial cell proliferation in the visceral pleura in mice and rats.^(14–16) However, deposition of MWCNT and induction of associated lesions in the parietal pleura have not been reported.

The pleural responses to fibrous particles that deposit in the pleural cavity depend on the size of the particle. Murphy

et al.⁽¹⁷⁾ reported that intrapleural injection of long (>15 μm) but not short (<4 μm) MWCNT caused persistent inflammation and fibrosis of the parietal pleura up to 24 weeks post-treatment. Similarly, Schinwald *et al.*⁽¹⁸⁾ reported that injection of silver nanofibers with different lengths into the pleural cavity showed a clear length threshold effect, indicating that fibers longer than 4 μm were pathogenic to the pleura.

The main purpose of the present study was to determine if the size and shape of inhaled MWCNT impact on deposition and associated lesion development in the parietal and visceral pleura. Two different MWCNT were chosen for this study: larger needle-like MWCNTs (MWCNT-L, $l = 8 \mu\text{m}$, $d = 150 \text{ nm}$) and smaller-sized MWCNT (MWCNT-S, $l = 3 \mu\text{m}$, $d = 15 \text{ nm}$) that form cotton candy-like aggregates. We gave relatively high doses (125 $\mu\text{g}/\text{rat} \times 13 \text{ doses}$) of the two MWCNT suspensions over a 24-week period to the rat lung by transtracheal intrapulmonary spraying (TIPS) in order to examine detectable fibers and associated inflammatory and proliferative lesions in the pleura.

Materials and Methods

Animals. Eight-week-old male F344 rats (Charles River, Kanagawa, Japan) were housed on a 12:12 h light:dark cycle and received Oriental MF basal diet (Oriental Yeast, Tokyo, Japan) and water *ad libitum*. The study was conducted according to the Guidelines for the Care and Use of Laboratory Animals of Nagoya City University Medical School (Nagoya, Japan) and the experimental protocol was approved by the Institutional Animal Care and Use Committee (H22M-19).

Preparation of MWCNT suspensions. We used two types of MWCNTs grown in the vapor phase. The larger-sized MWCNTs (MWCNT-L) had a primary mean length of 8 μm and a diameter of 150 nm, and the smaller-sized MWCNTs (MWCNT-S) had a primary mean length of 3 μm and a diameter of 15 nm. Five milligrams of MWCNT-L or MWCNT-S were suspended in 20 mL saline containing 0.5% Pluronic F68 (PF68, non-ionic, biocompatible amphiphilic block copolymers; Sigma-Aldrich, St. Louis, MO, USA) and homogenized for 1 min four times at 3000 rpm in a Polytron PT1600E benchtop homogenizer (Kinematika, Littau, Switzerland). The suspensions were sonicated for 30 min shortly before use to minimize aggregation. The concentration of MWCNTs was 250 $\mu\text{g}/\text{mL}$. The lengths of MWCNT-L in the suspensions were determined using a digital map meter (Comcurve-9 Junior; Koizumi Sokki, Nigata, Japan) on SEM photographs. Characterization of MWCNT including shape, elemental analysis, and size distribution is shown in Figure S1.

Transtracheal intrapulmonary spraying of MWCNTs into the lung and pleural cavity lavage. Spraying of MWCNT suspensions into the lung and pleural cavity lavage (PCL) were carried out as previously described.^(15,19) Ten-week-old male Fisher 344 rats were divided into four groups of six animals each. Group 1 did not receive any treatment, and Groups 2, 3, and 4 were given 0.5 mL saline containing 0.5% PF68 or 250 $\mu\text{g}/\text{mL}$ MWCNT-L or MWCNT-S suspensions by TIPS under anesthesia by isoflurane once every 2 weeks, 13 times over a 24-week period. The total amount of the MWCNT fibers given to Groups 3 and 4 was $13 \times 0.125 = 1.625 \text{ mg}/\text{rat}$. Twenty-four hours after the last TIPS, the rats were placed under deep isoflurane anesthesia and PCL was carried out. The rats were then killed by exsanguination from the inferior vena cava. The left lung was frozen in liquid nitrogen for biochemi-

cal analysis, and the right lung, as well as other major organs and lymph nodes, were processed for histological examination.

Light microscopy, polarized light microscopy, and SEM. The MWCNT fibers in H&E stained slides of lung tissue, PCL cell pellets, and chest wall sections were observed with polarized light microscopy (PLM, BX51N-31P-O; Olympus, Tokyo, Japan) at $\times 1000$ magnification. The exact localization of the illuminated fibers was confirmed in the same H&E stained sections after removing the polarizing filter.

For SEM, H&E stained slides were immersed in xylene for 2–3 days to remove the cover glass, immersed in 100% ethanol for 10 min to remove the xylene, and air-dried for 2 h at room temperature. The slides were then coated with platinum for viewing the MWCNT fibers by SEM (Model S-4700 Field Emission Scanning Electronic Microscope; Hitachi High Technologies, Tokyo, Japan) at 5–10 kV.

Azan–Mallory staining and measurement of the thickness of the parietal and visceral pleura. To clearly visualize collagen fibers in the lung and the pleura, Azan–Mallory staining was carried out using Azan staining reagents (Muto Pure Chemicals, Tokyo, Japan). The thickness of the pleura was measured on the basis of the Azan–Mallory stained sections (Fig. S2). For the rats treated with MWCNT-L, only the parietal and visceral pleural regions with observed MWCNT-L fibers by PLM were measured. Because obvious thickening of the pleura was not observed in the rats treated with PF68 or MWCNT-S, six pleural regions in each parietal and visceral pleura of each rat were randomly selected for measurement.

Analysis of inflammatory reaction in the pleural cavity. Cells in the lavage fluid were counted using a hemocytometer (Erma, Tokyo, Japan), and the cellular fraction was then isolated by centrifugation at 200g for 5 min at 4°C. To make cell pellets, cells collected from three rats were combined (generating a total of two cell pellets per group) and resuspended in 0.2 mL of 1% sodium alginate (Sigma-Aldrich) by pipetting. The suspension was then solidified by addition of one drop of 1 M CaCl_2 . The cell pellets were fixed in 4% paraformaldehyde and processed for histological examination. Total protein in the supernatants of each of the lavage fluids was determined using the Pierce BCA Protein Assay Kit (Thermo Fisher Scientific, Rockford, IL, USA). Cytokines and chemokines were analyzed as described below.

Analysis of cytokines and chemokines by Multiplex Suspension Array. Approximately 100 mg of the left lung tissues was rinsed with cold PBS three times and homogenized in 1 mL T-PER Tissue Protein Extraction Reagent (Pierce, Rockford, IL, USA), containing 1% (v/v) proteinase inhibitor cocktail (Sigma-Aldrich). The homogenates were clarified by centrifugation at 10 000 g for 5 min at 4°C. Protein content was measured as described above. The levels of 20 cytokines and chemokines (interleukin [IL]-1 α , IL-1 β , IL-2, IL-4, IL-6, IL-12 [p70], IL-17, IL-18, granulocyte/macrophage colony-stimulating factors [GM-CSF], granulocyte colony-stimulating factor [G-CSF], tumor necrosis factor [TNF]- α , γ -interferon, monocyte chemotactic protein [MCP]1, macrophage inflammatory protein [MIP]1 α , MIP2, interferon gamma-induced protein [IP]-10, regulated on activation, normal T cell expressed and secreted [RANTES], growth related oncogene/keratinocyte-derived cytokine [GRO/KC], vascular endothelial growth factor [VEGF], and epidermal growth factor [EGF]) in the lung tissue extracts and in the supernatants of the lavage fluids were measured by the Multiplex MAP Rat Cytokine/Chemokines Magnetic Bead Panel (Filgen, Nagoya, Japan).

Immunohistochemistry. CD68, proliferating cell nuclear antigen (PCNA), and mesothelin/Erc were detected using anti-rat CD68 antibodies (BMA Biomedicals, Augst, Switzerland), anti-

PCNA mAbs (Clone PC10; Dako Japan, Tokyo, Japan) and anti-rat C-ERC/mesothelin polyclonal antibodies (Immuno-Biological Laboratories, Gunma, Japan). The CD68, PCNA, and C-ERC/mesothelin antibodies were diluted 1:100, 1:200, and 1:1000, respectively, in blocking solution and applied to deparaffinized slides, and the slides were incubated at 4°C overnight. The slides were then incubated for 1 h with biotinylated species-specific secondary antibodies diluted 1:500 (Vector Laboratories, Burlingame, CA, USA) and visualized using avidin-conjugated HRP complex (ABC kit; Vector Laboratories).

Statistical analysis. Statistical analysis was carried out using ANOVA. Statistical significance was analyzed using two-tailed Student's *t*-test. A *P*-value of <0.05 was considered to be significant.

Results

Deposition of MWCNT-L in the pleura. Observation of the pleural tissue sections with PLM and SEM indicated that MWCNT-L deposited in the parietal pleura in four out of six rats, most of the fibers being located in fibrotic parietal pleura, with a few piercing and penetrating into the parietal mesothelium (Fig. 1a–c); MWCNT-L was also found in the visceral pleura (Fig. 1d–f).

Smaller sized MWCNT did not cause polarization and consequently were not detected by PLM (Fig. 1h,k); therefore, observation of MWCNT-S was made mainly by SEM. The MWCNT-S were not found in either the parietal (Fig. 1g–i) or visceral (Fig. 1j) pleura and were often found phagocytosed in alveolar macrophages close to the visceral pleura (Fig. 1j–l).

Fibrosis and mesothelial proliferation in the pleura. Deposition of MWCNT-L in the parietal and visceral pleura was preferen-

tially localized in thickened fibrotic lesions (Fig. 1a,d). Azan–Mallory staining indicated that the thickened lesions were composed of collagen fibers (Fig. 2a). The thickness of the parietal and visceral pleura with deposition of MWCNT-L was $28.75 \pm 10.43 \mu\text{m}$ and $18.92 \pm 10.13 \mu\text{m}$, respectively, both lesions showing a significant increase compared to those in the rats treated with MWCNT-S ($7.28 \pm 4.37 \mu\text{m}$ and $6.16 \pm 2.05 \mu\text{m}$) or with the dispersing agent, PF68, alone ($7.16 \pm 4.95 \mu\text{m}$ and $4.57 \pm 1.23 \mu\text{m}$; Fig. 2b). An increase in the thickness of the visceral pleura of the rats treated with MWCNT-S compared with the PF68-treated rats was also observed (Fig. 2b).

Neoplastic development was not found in the parietal or visceral pleura of either the MWCNT-L or MWCNT-S groups; however, in the MWCNT-L group, patchy foci of mesothelial cell proliferation were observed in the parietal pleura (Fig. 3a) and PCNA indices were significantly increased in both parietal and visceral mesothelium. The PCNA indices of the MWCNT-S group were comparable to those of the PF68 treated rats (Fig. 3b).

Translocation of MWCNT-L into the pleural cavity. In the cell pellets of the PCL, MWCNT-L was found with both PLM and SEM observations. Larger sized MWCNT fibers were observed mainly within and/or attached to the cell surface of macrophages (Fig. 4a). The ratio of the MWCNT-L containing macrophages to the total cell count was approximately 1:1800 and the average length of MWCNT-L was $6.23 \pm 4.11 \mu\text{m}$ (data not shown). Smaller sized MWCNT could not be detected (Fig. 4a).

Inflammation in the pleural cavity. Both MWCNT-L and MWCNT-S treatments caused inflammatory reactions in the

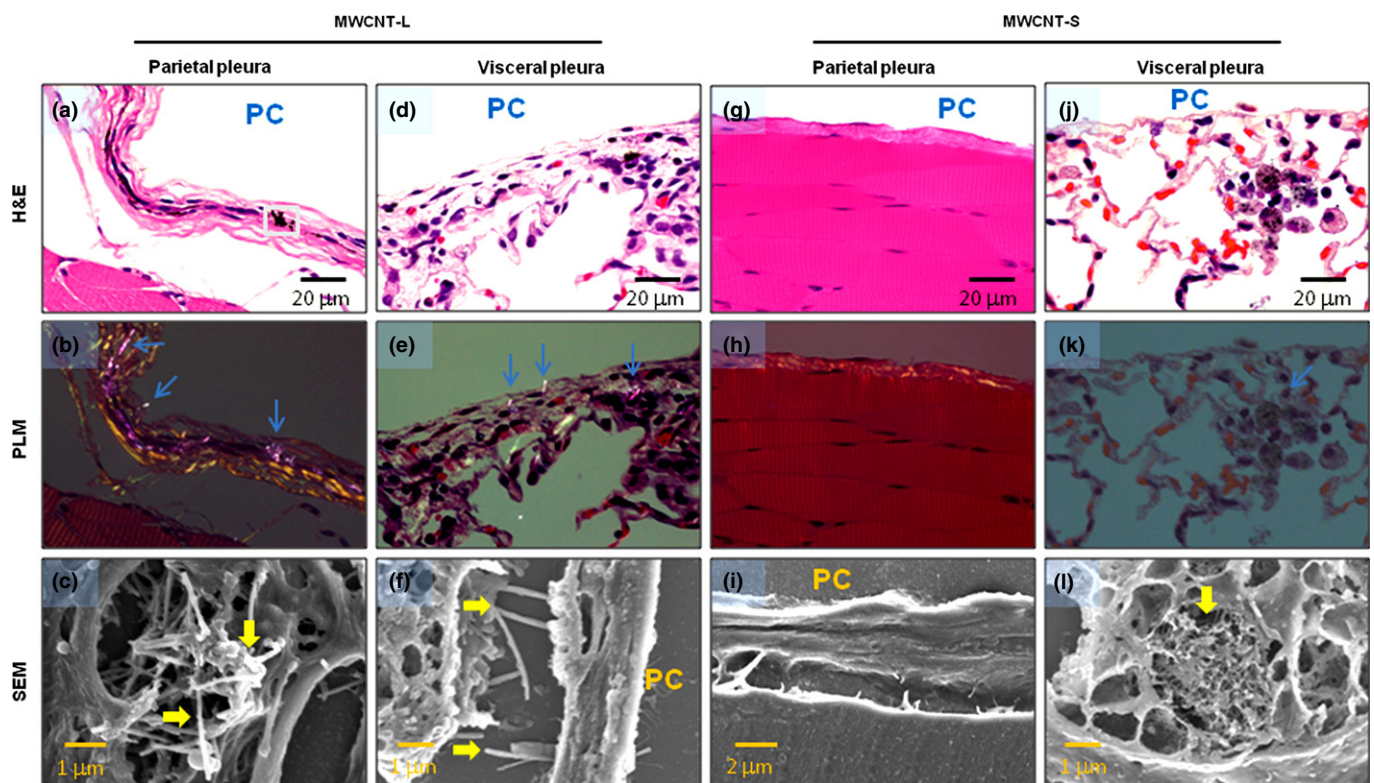


Fig. 1. Evidence of multiwalled carbon nanotube (MWCNT) fibers in the pleura. Existence of MWCNT fibers in the parietal (a–c, g–i) and visceral (d–f, j–l) pleura of rats treated with larger sized MWCNT (MWCNT-L; $l = 8 \mu\text{m}$, $d = 150 \text{ nm}$) (a–f) or smaller sized MWCNT (MWCNT-S; $l = 3 \mu\text{m}$, $d = 15 \text{ nm}$) (g–l) was examined by polarized light microscopy (PLM) (d, e, h, k) and SEM (c, f, i, l). The area in (a) denoted by the square was subjected to SEM observation, shown in (c). Arrows indicate MWCNT fibers. PC, pleural cavity.

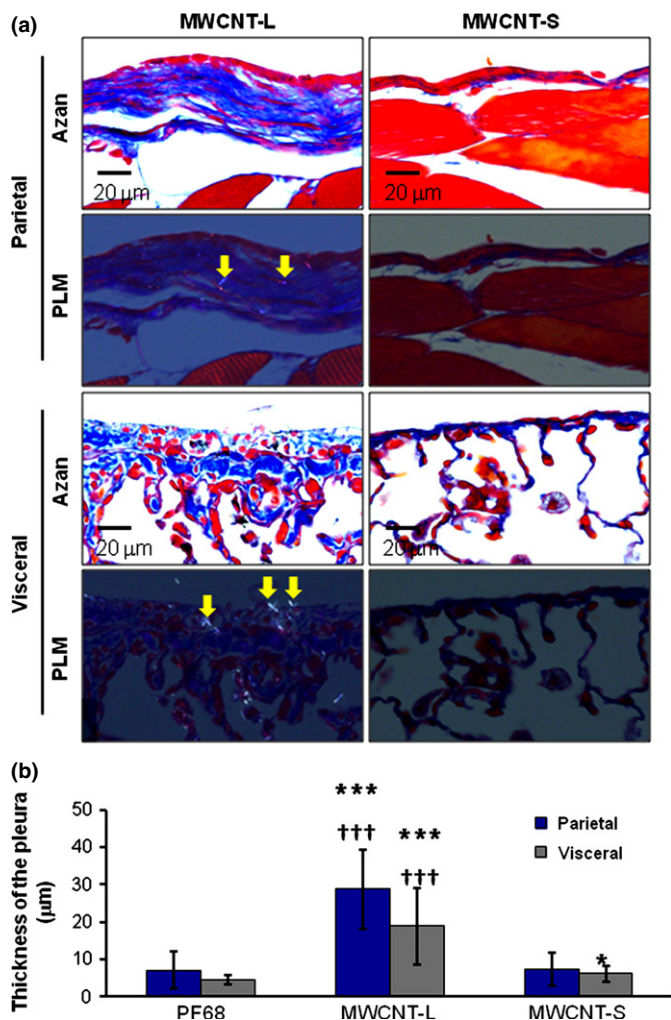


Fig. 2. Azan–Mallory (Azan) staining and thickness of the parietal and visceral pleura. (a) Azan–Mallory staining images and polarized light microscopy (PLM) images of the parietal and visceral pleura in rats sprayed with larger sized multiwalled carbon nanotubes (MWCNT-L; $l = 8 \mu\text{m}$, $d = 150 \text{ nm}$) or smaller sized MWCNT (MWCNT-S; $l = 3 \mu\text{m}$, $d = 15 \text{ nm}$). (b) Quantification of the thickness of the parietal and visceral pleura of rats treated with Pluronic F68 (PF68), MWCNT-L, or MWCNT-S on the basis of Azan–Mallory stained images. $*P < 0.05$ versus PF68; $***P < 0.001$ versus PF68; $†††P < 0.001$ MWCNT-L versus MWCNT-S by two-tailed Student's t -test. Arrows indicate MWCNT fibers.

pleural cavity. In the PCL, the total cell number, composed mostly of macrophages, neutrophils, eosinophils, and lymphocytes, in the MWCNT-L and MWCNT-S treated groups was significantly increased compared with the PF68 group. The PCL cell number in the MWCNT-L group was significantly greater than in the MWCNT-S group (Fig. 4b). A similar pattern was observed for the ratio of cells positive for CD-68, a macrophage/monocyte marker (Fig. 4c). The ratios of cells in the PCL pellets positive for mesothelin/Erc, a mesothelial cell marker, were approximately 1%, indicating that the increased cell number in the pleural cavity of the rats treated with MWCNT-L and MWCNT-S was caused by inflammatory cell effusion, not by mesothelial cell shedding from the mesothelium. Treatment with MWCNT-L also caused an increase in the total protein level of the cell-free PCL (Fig. 4d). Analysis

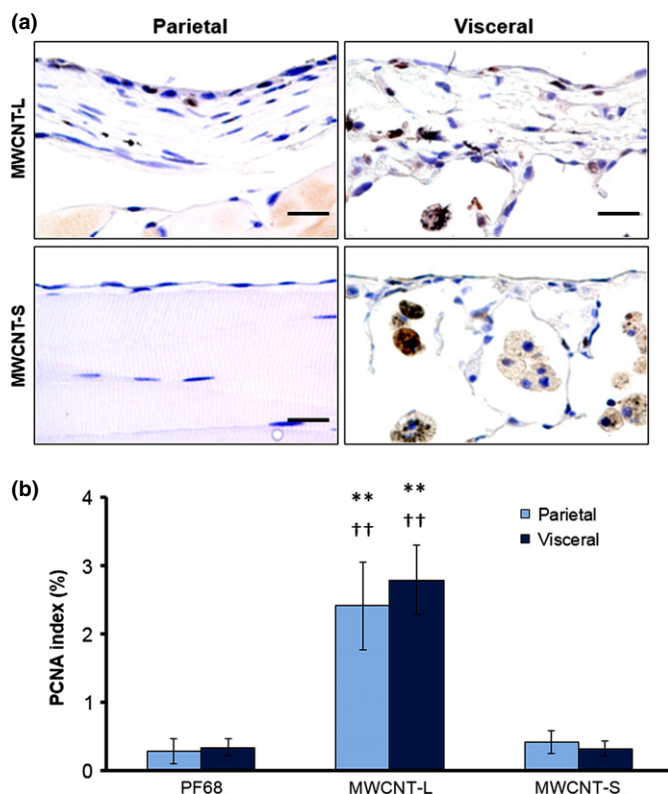


Fig. 3. Cell proliferation of the parietal and visceral mesothelium. (a) Representative proliferating cell nuclear antigen (PCNA) immunostained images of the parietal and visceral pleural regions of rats treated with larger sized multiwalled carbon nanotubes (MWCNT-L; $l = 8 \mu\text{m}$, $d = 150 \text{ nm}$) or smaller sized MWCNT (MWCNT-S; $l = 3 \mu\text{m}$, $d = 15 \text{ nm}$). (b) PCNA indices (percentages of PCNA positive mesothelial cells in total mesothelial cells). Scale bar = $20 \mu\text{m}$. $**P < 0.01$ versus Pluronic F68 (PF68); $††P < 0.01$ MWCNT-L versus MWCNT-S.

of 20 cytokines and chemokines by Multiplex Suspension Array indicated that the levels of IP-10, RANTES, IL-2, and IL-18 were significantly higher in the MWCNT-L group than the MWCNT-S group (Table 1).

Toxicological responses in the lung. In the lung tissue, both MWCNT-L and MWCNT-S treatments induced small granulation foci and scattered infiltration of macrophages in the alveoli (Fig. S3A,B). Alveolar neoplastic proliferation was not found. The number of alveolar macrophages was higher in the MWCNT-S group than in the MWCNT-L group. We were unable to quantitatively analyze the alveolar macrophage number, because most of the alveolar macrophages induced by MWCNT-S were degenerative or necrotic. Most of the MWCNT-L fibers were found within alveolar macrophages (Fig. S3C), with a few penetrating the alveolar epithelium (Fig. S3D), whereas MWCNT-S fibers were observed in alveolar macrophages, but not in the alveolar epithelium (Fig. S3E). Multiplex Suspension Array analysis of 20 cytokines and chemokines in the lung tissue indicated that the levels of MIP1 α , MIP2, MCP1, IP10, IL-1 β , IL-18, and VEGF were significantly higher in the MWCNT-S group than in the MWCNT-L group; the values of GRO/KC and IL-1 α were elevated in both the MWCNT-L and MWCNT-S treated groups without an intergroup difference. The level of RANTES was significantly higher in the MWCNT-L group than the MWCNT-S group, and the other 10 cytokines were compara-

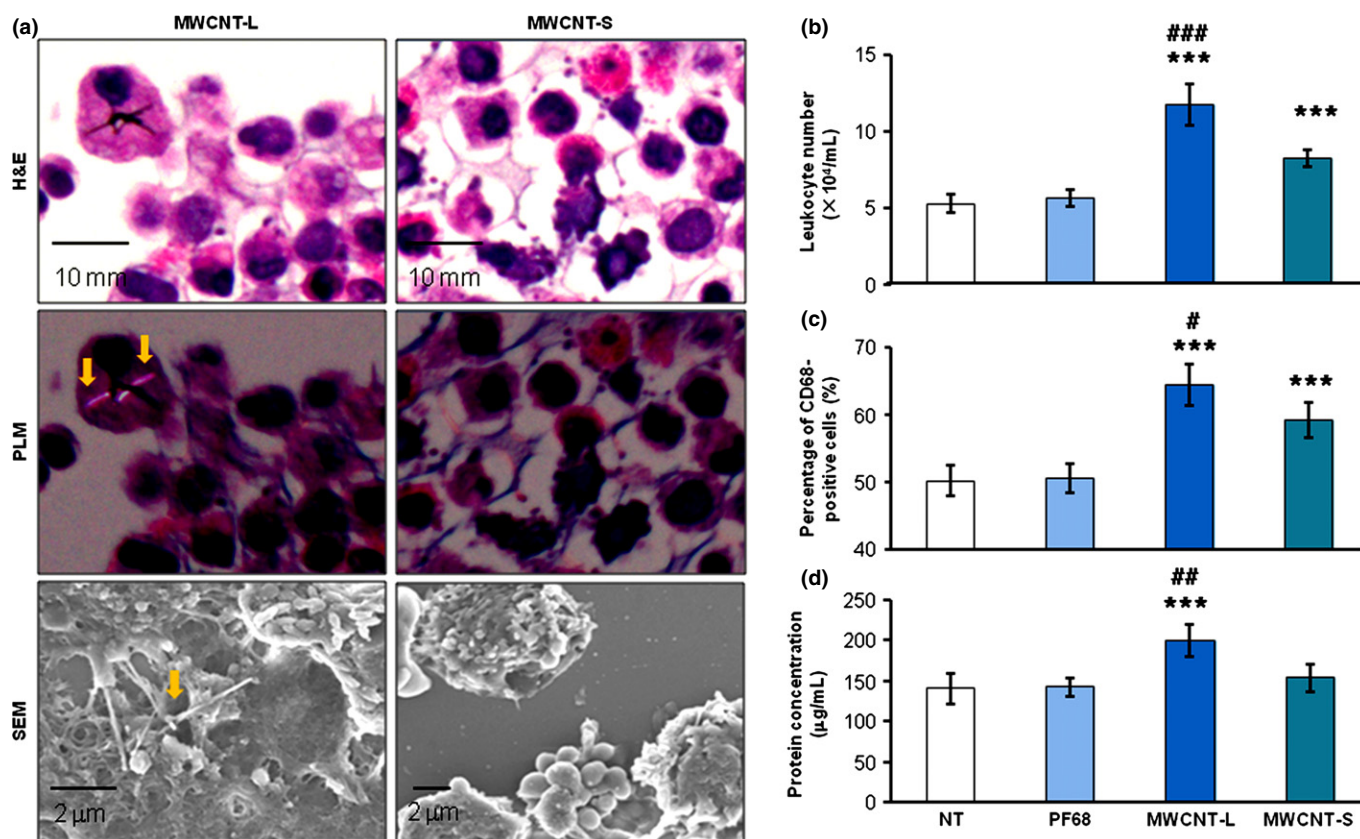


Fig. 4. Demonstration of multiwalled carbon nanotube (MWCNT) fibers and analysis of inflammatory reactions in the pleural cavity. (a) H&E staining, polarized light microscopy (PLM), and SEM images of pleural cell pellets taken from rats treated with larger sized MWCNT (MWCNT-L; $l = 8 \mu\text{m}$, $d = 150 \text{ nm}$) or smaller sized MWCNT (MWCNT-S; $l = 3 \mu\text{m}$, $d = 15 \text{ nm}$). Arrows indicate MWCNT fibers. (b–d) Analysis of leukocyte number (b), proportion of CD 68-positive cells (c), and protein concentration (d) in the supernatants of pleural cavity lavages. $***P < 0.001$ versus Pluronic F68 (PF68); $\#P < 0.05$, $\#\#P < 0.01$, and $\#\#\#P < 0.001$ MWCNT-L versus MWCNT-S by two-tailed Student's *t*-test. NT, no treatment.

ble among the PF68, MWCNT-L, and MWCNT-S treated groups (Table 1). Smaller sized MWCNT were more potent than MWCNT-L in inducing 8-hydroxydeoxyguanosine (8-OHdG), a marker for oxidative stress, in the lung tissue (Fig. S3F).

Transportation of MWCNT-L to extrapulmonary organs. In addition to the lung and pleura, MWCNT-L was found in extrapulmonary organs. Polarized light microscopy observations indicated that MWCNT-L was transported to the mediastinal (Fig. S4A), submandibular (Fig. S4B), and mesentery (Fig. S4C) lymph nodes, with many more fibers in the mediastinal lymph nodes than in the other examined lymph nodes. A few MWCNT-L fibers were also observed in the liver (Fig. S4D), kidney (Fig. S4E), spleen (Fig. S4F), and brain (Fig. S4G). Examination with SEM did not detect MWCNT-S in these organs.

Cytotoxicity *in vitro*. Smaller sized MWCNT were more potent than MWCNT-L in lowering cell viability of primary rat alveolar macrophages, human mesothelioma cells, human lung carcinoma cells, and human lung fibroblasts *in vitro* (Fig. S5).

Discussion

Multiwalled carbon nanotubes, when injected into the peritoneal cavity or the scrotum, results in the development of mesothelioma.^(11–13) It is of great interest to know whether

pulmonary exposure leads to migration of MWCNT into the pleural cavity. Our previous study showed that short-term exposure of the lung to MWCNT resulted in fiber translocation into the pleural cavity and induction of pleural inflammation and fibrosis and mesothelial cell proliferation in the visceral pleura.⁽¹⁵⁾ Similarly, Porter *et al.* and Mercer *et al.* showed that MWCNT could reach the visceral pleura⁽²⁰⁾ and enter the pleural cavity.⁽¹⁴⁾ Furthermore, Mercer *et al.*⁽¹⁶⁾ showed that MWCNT was transported to the muscle tissue of the chest wall and distant organs. Multiwalled carbon nanotubes were not found in the parietal pleura in these studies, probably due to short exposure periods and/or low doses.

Development of asbestos-induced pleural malignant mesothelioma in humans is a long-term process with a latency of up to tens of years,⁽²⁾ indicating this is a cumulative effect of the fibers and associated pathogenic responses in the pleura. Thus, accurate modeling of human exposure to asbestos-like fibers and related pathogenesis in rodents is difficult. One solution to this problem is to increase exposure doses in animals. Therefore, in the present study, we sprayed a relatively high dose of MWCNT into the rat lung for a longer exposure period. The dosing was much higher than the recommended exposure limit of $1 \mu\text{g}/\text{m}^3$ to carbon nanotubes and carbon nanofibers for an 8-h time-weight average proposed by the US National Institute of Occupational Safety and Health in 2013 (<http://www.cdc.gov/niosh/docs/2013-145/>).

Table 1. Cytokines/chemokines in the pleural cavity lavage and lung tissue of rats treated with multiwalled carbon nanotubes (MWCNT)

Cytokines/chemokines	Pleural cavity lavage (pg/mL)			Lung tissue (pg/mg protein)		
	PF68	MWCNT-L	MWCNT-S	PF68	MWCNT-L	MWCNT-S
G-CSF	n.d.	n.d.	n.d.	n.d.	n.d.	n.d.
GM-CSF	n.d.	n.d.	n.d.	n.d.	n.d.	n.d.
MIP1 α	n.d.	n.d.	n.d.	63.8 \pm 16.2	120.7 \pm 21.0***	331.5 \pm 90.4***,†††
MIP2	n.d.	n.d.	n.d.	12.4 \pm 6.1	27.2 \pm 4.9***	59.7 \pm 16.7***,††
MCP1	n.d.	n.d.	n.d.	18.0 \pm 13.9	39.1 \pm 16.3*	213.1 \pm 45.8***,†††
TNF- α	n.d.	n.d.	n.d.	n.d.	n.d.	n.d.
IFN- γ	n.d.	n.d.	n.d.	n.d.	n.d.	n.d.
GRO/KC	n.d.	n.d.	n.d.	425.2 \pm 194.3	1105.4 \pm 395.7**	1353.1 \pm 362.6***
IP10	1.5 \pm 1.5	8.9 \pm 2.3***,†††	2.3 \pm 2.3	35.6 \pm 5.8	49.9 \pm 4.4***	64.0 \pm 11.0***,†
RANTES	3.8 \pm 0.9	6.9 \pm 1.9***,†††	4.1 \pm 0.7	556.0 \pm 128.6	531.7 \pm 127.9††	335.4 \pm 61.3**
IL-1 α	n.d.	n.d.	n.d.	56.9 \pm 14.4	85.3 \pm 7.3**	84.5 \pm 14.0**
IL-1 β	n.d.	n.d.	n.d.	73.0 \pm 19.3	103.7 \pm 18.6*	154.5 \pm 17.6***,†††
IL-4	n.d.	n.d.	n.d.	3.7 \pm 3.0	4.2 \pm 3.4	3.8 \pm 1.9
IL-2	1.2 \pm 1.9	14.1 \pm 5.5***,††	5.2 \pm 5.9	18.3 \pm 4.1	18.9 \pm 3.0	20.3 \pm 7.7
IL-6	n.d.	n.d.	n.d.	29.1 \pm 14.1	27.0 \pm 13.5	32.6 \pm 13.4
IL-12p70	n.d.	n.d.	n.d.	n.d.	n.d.	n.d.
IL-17 α	n.d.	n.d.	n.d.	n.d.	n.d.	n.d.
IL-18	66.3 \pm 17.0	108.4 \pm 25.1**,†	70.4 \pm 21.5	2294.8 \pm 495.2	2471.8 \pm 391.7	3085.6 \pm 418.4*,†
VEGF	n.d.	n.d.	n.d.	111.0 \pm 24.0	99.1 \pm 14.4	201.4 \pm 13.8***,†††
EGF	n.d.	n.d.	n.d.	n.d.	n.d.	n.d.

Data are expressed as mean \pm standard deviation, $n = 6$ in each treatment group. * $P < 0.05$, ** $P < 0.01$, *** $P < 0.001$, larger sized MWCNT (MWCNT-L; $l = 8 \mu\text{m}$, $d = 150 \text{ nm}$) or smaller sized MWCNT (MWCNT-S; $l = 3 \mu\text{m}$, $d = 15 \text{ nm}$) versus Pluronic F68 (PF68). † $P < 0.05$, †† $P < 0.01$, ††† $P < 0.001$, MWCNT-L versus MWCNT-S. EGF, epidermal growth factor; G-CSF, granulocyte colony-stimulating factor; GM-CSF, granulocyte/macrophage colony-stimulating factor; GRO/KC, growth related oncogene/keratinocyte-derived cytokine; IFN γ , γ -interferon; IL, interleukin; IP-10, interferon gamma-induced protein 10; n.d., not detectable; TNF- α , tumor necrosis factor- α ; MCP1, monocyte chemoattractant protein 1; MIP, macrophage inflammatory protein; RANTES, regulated on activation, normal T cell expressed and secreted; VEGF, vascular endothelial growth factor.

The results of this study show that MWCNT-L applied to the lung was found in the pleural cavity and deposited in the parietal pleura, and induced higher inflammatory reactions in the pleural cavity, fibrotic thickening of both the parietal and visceral pleura, and mesothelial proliferation, whereas MWCNT-S caused higher inflammatory reactions and 8-OHdG formation in the lung. Reports have shown that pro-inflammatory cytokines promote mesothelial cell transformation *in vitro*,⁽²¹⁾ indicating chronic inflammation is a likely contributing factor in the development of mesothelioma. Due to its length and needle-like shape, MWCNT-L deposited in the pleura, especially in the parietal side, is difficult to clear and results in chronic inflammation in the deposited site. Thus, MWCNT-L has more potential to cause pleural mesothelioma.

It should be noted that properties of MWCNT-L and MWCNT-S, other than size and shape, such as chemical composition (MWCNT-L contains zinc [Fig. S1]) and rigidity,⁽²²⁾ may contribute to the observed different effects in the pleura and lung. Smaller sized MWCNT were not found in the pleural cavity, possibly because MWCNT-S formed cotton candy-like aggregates and very few free fibers translocated from the lung to the pleural cavity, or/and these fibers were rapidly cleared from the pleural cavity. The size- and shape-dependent pleural toxicity shown in our study is consistent with previous reports that direct injection of MWCNT into the pleural cavity leads to length-dependent retention of MWCNT in the pleural cavity and sustained inflammation and fibrosis in the parietal pleura,⁽¹⁷⁾ and with reports that inhaled amosite fibers are found in the parietal pleura with inflammation and fibrosis.^(23,24) When we were preparing this manuscript, Murphy *et al.* reported that long MWCNT aspired into the lung of

mice was found in the parietal pleura and caused stronger inflammation and fibrosis both in the pleura and lung than short or tangled MWCNT. The lung responses to short or tangled MWCNT are different from our results, possibly due to different animals, administration methods, MWCNT used, and sampling time.⁽²⁵⁾

Current administration regulations to set permissible air concentrations of particles and fibers are usually based on lung burdens. Although lung diseases may well be related to the lung burden of specific particles or fibers, lung burden is not always suitable for prediction of pleural toxicity of asbestos-like materials.^(2,7) In the present study, MWCNT-S showed higher toxicity in the lung, whereas MWCNT-L was more toxic in the pleural tissue, indicating that the site of deposition and the associated toxicity needs to be taken into account in regulating carbon nanotube exposure.

In conclusion, deposition of MWCNT-L and induction of fibrosis and mesothelial cell proliferation in the parietal pleura indicate that larger sized MWCNT has greater potential to induce asbestos-like pleural lesions.

Acknowledgments

This work was supported by Health and Labor Sciences Research Grants of Japan (Research on Risk of Chemical Substance 21340601, grant nos. H22-kagaku-ippan-005, H24-kagaku-sitei-009, and H25-kagaku-ippan-004) and by the Princess Takamatsu Cancer Research Fund (H24).

Disclosure Statement

The authors have no conflict of interests.

References

- 1 Boutin C, Rey F, Gouvernet J, Viallat JR, Astoul P, Ledoray V. Thoracoscopy in pleural malignant mesothelioma: a prospective study of 188 consecutive patients. Part 2: prognosis and staging. *Cancer* 1993; **72**: 394–404.
- 2 Cugell DW, Kamp DW. Asbestos and the pleura: a review. *Chest* 2004; **125**: 1103–17.
- 3 Kane AB. Mechanisms of mineral fibre carcinogenesis. *IARC Sci Publ* 1996; **140**: 11–34.
- 4 Robinson BW, Musk AW, Lake RA. Malignant mesothelioma. *Lancet* 2005; **366**: 397–408.
- 5 Boutin C, Dumortier P, Rey F, Viallat JR, De Vuyst P. Black spots concentrate oncogenic asbestos fibers in the parietal pleura. Thoracoscopic and mineralogic study. *Am J Respir Crit Care Med* 1996; **153**: 444–9.
- 6 Kohyama N, Suzuki Y. Analysis of asbestos fibers in lung parenchyma, pleural plaques, and mesothelioma tissues of North American insulation workers. *Ann N Y Acad Sci* 1991; **643**: 27–52.
- 7 Donaldson K, Murphy FA, Duffin R, Poland CA. Asbestos, carbon nanotubes and the pleural mesothelium: a review of the hypothesis regarding the role of long fibre retention in the parietal pleura, inflammation and mesothelioma. *Part Fibre Toxicol* 2010; **7**: 5.
- 8 Bonner JC. Nanoparticles as a potential cause of pleural and interstitial lung disease. *Proc Am Thorac Soc* 2010; **7**: 138–41.
- 9 Nagai H, Toyokuni S. Biopersistent fiber-induced inflammation and carcinogenesis: lessons learned from asbestos toward safety of fibrous nanomaterials. *Arch Biochem Biophys* 2010; **502**(1): 1–7.
- 10 Poland CA, Duffin R, Kinloch I *et al.* Carbon nanotubes introduced into the abdominal cavity of mice show asbestos-like pathogenicity in a pilot study. *Nat Nanotechnol* 2008; **3**: 423–8.
- 11 Sakamoto Y, Nakae D, Fukumori N *et al.* Induction of mesothelioma by a single intrascrotal administration of multi-wall carbon nanotube in intact male Fischer 344 rats. *J Toxicol Sci* 2009; **34**(1): 65–76.
- 12 Takagi A, Hirose A, Futakuchi M, Tsuda H, Kanno J. Dose-dependent mesothelioma induction by intraperitoneal administration of multi-wall carbon nanotubes in p53 heterozygous mice. *Cancer Sci* 2012; **103**: 1440–4.
- 13 Takagi A, Hirose A, Nishimura T *et al.* Induction of mesothelioma in p53^{+/-} mouse by intraperitoneal application of multi-wall carbon nanotube. *J Toxicol Sci* 2008; **33**: 105–16.
- 14 Mercer RR, Hubbs AF, Scabilloni JF *et al.* Distribution and persistence of pleural penetrations by multi-walled carbon nanotubes. *Part Fibre Toxicol* 2010; **7**: 28.
- 15 Xu J, Futakuchi M, Shimizu H *et al.* Multi-walled carbon nanotubes translocate into the pleural cavity and induce visceral mesothelial proliferation in rats. *Cancer Sci* 2012; **103**: 2045–50.
- 16 Mercer RR, Scabilloni JF, Hubbs AF *et al.* Extrapulmonary transport of MWCNT following inhalation exposure. *Part Fibre Toxicol* 2013; **10**(1): 38.
- 17 Murphy FA, Poland CA, Duffin R *et al.* Length-dependent retention of carbon nanotubes in the pleural space of mice initiates sustained inflammation and progressive fibrosis on the parietal pleura. *Am J Pathol* 2011; **178**: 2587–600.
- 18 Schinwald A, Murphy FA, Prina-Mello A *et al.* The threshold length for fiber-induced acute pleural inflammation: shedding light on the early events in asbestos-induced mesothelioma. *Toxicol Sci* 2012; **128**: 461–70.
- 19 Xu J, Futakuchi M, Iigo M *et al.* Involvement of macrophage inflammatory protein 1alpha (MIP1alpha) in promotion of rat lung and mammary carcinogenic activity of nanoscale titanium dioxide particles administered by intrapulmonary spraying. *Carcinogenesis* 2010; **31**: 927–35.
- 20 Porter DW, Hubbs AF, Mercer RR *et al.* Mouse pulmonary dose- and time course-responses induced by exposure to multi-walled carbon nanotubes. *Toxicology* 2010; **269**: 136–47.
- 21 Wang ZL. Functional oxide nanobelts: materials, properties and potential applications in nanosystems and biotechnology. *Annu Rev Phys Chem* 2004; **55**: 159–96.
- 22 Nagai H, Okazaki Y, Chew SH *et al.* Diameter and rigidity of multiwalled carbon nanotubes are critical factors in mesothelial injury and carcinogenesis. *Proc Natl Acad Sci U S A* 2011; **108**: E1330–8.
- 23 Bernstein DM, Rogers RA, Sepulveda R *et al.* The pathological response and fate in the lung and pleura of chrysotile in combination with fine particles compared to amosite asbestos following short-term inhalation exposure: interim results. *Inhal Toxicol* 2010; **22**: 937–62.
- 24 Bernstein DM, Rogers RA, Sepulveda R *et al.* Quantification of the pathological response and fate in the lung and pleura of chrysotile in combination with fine particles compared to amosite-asbestos following short-term inhalation exposure. *Inhal Toxicol* 2011; **23**: 372–91.
- 25 Murphy FA, Poland CA, Duffin R, Donaldson K. Length-dependent pleural inflammation and parietal pleural responses after deposition of carbon nanotubes in the pulmonary airspaces of mice. *Nanotoxicology* 2013; **7**: 1157–67.

Supporting Information

Additional supporting information may be found in the online version of this article:

Fig. S1. Characterization of multiwalled carbon nanotubes.

Fig. S2. Determination of the thickness of the pleura in rats treated with multiwalled carbon nanotubes.

Fig. S3. Granuloma formation, alveolar macrophage infiltration, and 8-hydroxydeoxyguanosine (8-OHdG) induction in the lung.

Fig. S4. Transportation of larger sized multiwalled carbon nanotubes to extrapulmonary organs.

Fig. S5. Cytotoxicity of multiwalled carbon nanotubes *in vitro*.